Welding in the World
https://doi.org/10.1007/s40194-023-01567-7

RESEARCH PAPER

Influence of edge-deposited layers on mechanical and corrosion properties of laser beam welds of 15 mm thick AISI 2205 duplex stainless steel

Anne Straße[1] · **Andrey Gumenyuk**[1,2] · **Michael Rethmeier**[1,2,3]

Received: 16 March 2023 / Accepted: 18 July 2023

Abstract
AISI 2205 duplex stainless steel is used in a variety of industries, including the chemical and petrochemical industries. This is due to its high tensile strength combined with good ductility and corrosion resistance. However, in laser beam welding, these properties are negatively affected by the high cooling rates typical of the welding process. The resulting higher ferrite content in the weld metal than in the base material leads to a reduction in the ductility and corrosion resistance of the welded joint. To overcome this problem, in this study, thick plates were coated by direct energy deposition (DED) prior to laser beam welding, whereas a duplex powder mixture containing a higher nickel concentration was used as a coating material. To improve the weld quality for the proposed two-step process, a method of additional material deposition instead of conventional tack weld was investigated. The resulting welded joints showed a well-balanced austenite to ferrite ratio and their properties and microstructure were verified by metallographic analysis, electron backscatter diffraction and Charpy impact testing. Using the standard ASTM G48 test method, it was found that the corrosion resistance of the welds was improved by a factor of four in average compared to the conventionally welded joints. The resulting properties, such as good ductility and corrosion resistance, of the welds with pre-coated edges showed good agreement with those of the base metal and confirmed the proposed two-step process as a promising alternative to the conventional approaches for welding thick duplex stainless steel plates.

Keywords Direct energy deposition by laser beam · Laser metal deposition · Laser beam welding · Stainless steel · Duplex AISI 2205

1 Introduction

Duplex stainless steels are characterised by a microstructure containing balanced amounts of austenite and ferrite, thus combining the properties of both constitutional phases. They offer the high tensile strength typical of ferritic steels, while retaining the good ductility and superior corrosion resistance of austenitic steels. These properties make them suitable for many industrial applications, such as pulp and paper, chemical tankers and petrochemicals [1]. A great challenge while welding these materials is maintaining the balance between ferritic and austenitic phases in the weld metal and heat affected zone (HAZ). Laser beam welding characterised by high cooling rates results in welds with up to 90% ferrite content, as reported by Kotecki [2]. He showed that this phenomenon occurs at relatively high cooling rates typical of

Recommended for publication by Commission IV - Power Beam Processes

✉ Anne Straße
anne.strasse@bam.de

[1] Department 9.3-Welding Technology, Bundesanstalt für Materialforschung und-prüfung (BAM), Unter den Eichen 87, 12205 Berlin, Germany

[2] Joining and Coating Division, Fraunhofer Institute for Production Systems and Design Technology, Pascalstraße 8-9, 10587 Berlin, Germany

[3] Institute of Machine Tools and Factory Management, Technische Universität Berlin, Pascalstraße 8-9, 10587 Berlin, Germany

Published online: 29 July 2023

laser beam welding. The austenitic phase does not have time to transform from ferrite during the short cooling, resulting in an unbalanced phase distribution and thus degraded properties in the welds. If the ferritic phase becomes dominating in a duplex steel weld joint microstructure, welds have a higher susceptibility to pitting corrosion and reduced ductility compared to the base material. One of the reasons for the poor corrosion resistance is the formation of Cr_2N reported by Hoffmeister et al. [3]. Nevertheless, laser beam welding has many advantages, such as the ability to weld thick plates in a single pass, high welding speed, low energy input and low distortion. In comparison, arc welding processes require multiple passes, resulting in repeated reheating of the parts and the possibility of the formation of unwanted secondary phases, such as sigma and chi phases, and a wide heat affected zone [4]. These aspects have led to industrial interest in laser beam welding of duplex steels, and various approaches have been investigated in the past to overcome these problems. Zambon and Bonollo [5] showed the positive influence of a higher $t_{12/8}$ time on the microstructure and the formation of the austenitic phase.

Capello et al. [6] treated the weld surface with a laser beam to achieve a higher austenite content in the weld material, while Young et al. [7] investigated the positive influence of post-weld heat treatment on phase evolution and mechanical properties. In particular, the latter two approaches work well for thin plates but offer no solution for thicker materials. In both studies, the plate thickness was 5 mm. Capello et al. [6] determined a maximum depth of 1.5 mm for the surface treatment and thus the depth of higher austenite content, resulting in welds with a balanced microstructure on the surface but inconsistent properties throughout the depth of the plate. Heat treatment, on the other hand, is a common approach to influence the austenite content throughout the weld and improve mechanical properties. Muthupandi et al. [8] studied its influence on gas tungsten arc welds compared to electron beam welds for 5 mm thick plates and achieved almost the same austenite content as in the base material. However, it is a time-consuming process and carries the risk of precipitation of sigma and chi phases in case of improper heat treatment regimes, resulting in reduced pitting resistance and toughness, as shown by Deng et al. [9] for different heat treatment temperatures. Nilsson [10] puts the temperature range for the appearance of both phases between 600 and 1000 °C. Dissolution of these unwanted secondary phases is possible, but requires temperatures above this interval. This results in a heat treatment of the entire welded part to avoid exposure of any region to the critical temperature range, and is limited by the size of the furnace. Another approach was based on the findings of van Nassau et al. [11], who recommended the use of nitrogen as a shielding gas for arc welding processes, since it acts as a stabiliser of the austenitic phase and thus helps to increase the austenite content in the weld. Keskitalo et al. [12] investigated its positive influence on laser beam welding processes for different types of duplex stainless steels. The same effect has been established by Baghdadchi et al. [13] for laser beam welding. Lai et al. [14] also confirmed the effects of pure nitrogen as a shielding gas for both the top and root side in the formation of austenite for laser beam welding, thereby improving corrosion resistance. Another approach has been to use filler materials, e.g. in the form of wire, foil or powder, with a higher nickel content. Nickel produces higher austenite ratios by extending the austenitic field to higher temperatures and thus initiating earlier ferrite-austenite transformation [15]. Muthupandi et al. [16] investigated these filler materials for laser and electron beam welding processes, while Wu et al. [17] used a powder nozzle to inject nickel powder into the melt pool.

However, the use of filler materials in the laser welding of thick plates can result in another problem. Gook et al. [18] showed for hybrid laser arc welding (HLAW) processes that filler materials are not uniformly transported through the weld. Their influence decreases with increasing plate thickness and at a depth of 14 mm or more, their elements are no longer detectable in the root of the weld. This results in welds with different properties at different depths and therefore unpredictable mechanical behaviour. A solution to this problem has been proposed by Westin et al. [19]. They used nickel foils to ensure uniform nickel distribution in the weld. These foils were placed between the joint parts prior to laser beam welding. A disadvantage is that the handling of the foils is cumbersome and time consuming.

Having been used for a long time for cladding parts with wear and corrosion resistant layers [20] and repair welding, e.g. the tips of turbine blades [21], direct energy deposition with a laser beam (DED-LB) has become increasingly important in recent years as an effective method for additive manufacturing of new components. The DED-LB process allows a large freedom of cladding directions with the possibility of high deposition rates as well as a relatively easy combination of different materials. The metal cladding powders can either be pre-mixed or combined during the process, which even allows the production of components with graded material compositions [22]. For laser beam welding of thick duplex plates, a two-step process was proposed by [23], where the first

step consisted of edge cladding of the plates by DED-LB with a powder mixture containing duplex stainless steel and nickel. The second step was laser beam welding of these clad edges. The authors were able to demonstrate the positive effect on impact toughness. This paper presents further and more detailed investigations of the welding process, the resulting microstructures and the mechanical properties.

2 Experimental setup

2.1 Materials

The base plates were duplex stainless steel AISI 2205 with the dimensions of 300 mm × 100 mm × 15 mm. The edge cladding of the base plates was done with a pre-mixed powder containing duplex steel AISI 2205 as a base with a grain size of 53–250 µm and pure nickel with a grain size of 45–125 µm. The chemical composition of all used materials is shown in Table 1. The powder mixture contained a total amount of 12% nickel.

2.2 Cladding equipment

For the edge cladding, a laser cell with a five-axis system (TruLaser Cell 3000, Trumpf) was used. The laser cell is equipped with a 16 kW Yb:YAG-disk laser (TruDisk 16002, Trumpf) with a wavelength of 1030 nm and a three-jet nozzle with a working distance of 16 mm. The powder was supplied by a powder feeder (Flowmotion Twin, Medicoat) with a helium as a carrying gas at a flow rate of 4 l·min^{-1}. The experimental setup for coating the joint parts is shown in Fig. 1.

To ensure a better coverage of the edges with shielding gas and thus a reduction of oxidation, extension sheets were fixed 1 to 2 mm beneath the surface edge of the upper base plate side. The cladding was performed as a single layer with a bidirectional strategy for subsequent tracks with the following parameters: a powder mass flow of 15 g·min^{-1}, a laser spot diameter of 1.6 mm, a laser power of 0.8 kW and a welding speed of 0.8 m·min^{-1}. Argon was used as the shielding gas for all samples at a flow rate of 10 l·min^{-1}.

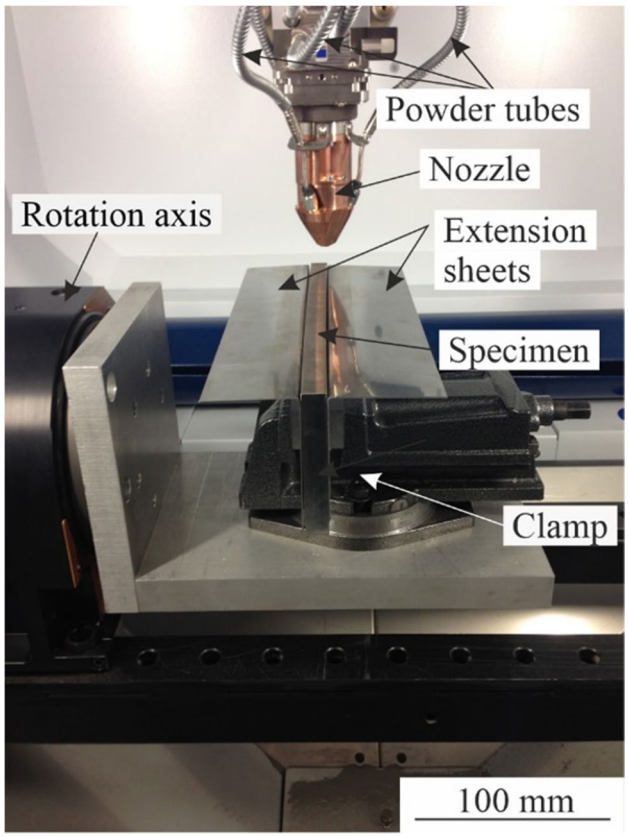

Fig. 1 Experimental setup for the edge coating

2.3 Welding equipment

The specimens were welded with a 20 kW Yb-fibre laser (YLR-20000, IPG) having a wavelength of 1064 nm, an optical fibre with a core diameter of 200 µm and a beam parameter product of 11.2 mm·mrad. The laser processing head (BIMO HP, HIGHYAG) with a focal length of 350 mm has focused the laser beam in a spot with a diameter of 0.56 mm. This was mounted at the arm of 6-axis robot (Kuka). The protection of the molten pool was realised by nitrogen as a shielding gas at different flow rates. A shielding gas nozzle (approx. 25 l·min^{-1}), a dragging nozzle (35 l·min^{-1}) and a root shielding nozzle (50 l·min^{-1}) were used. The following welding parameters have been used: The laser power of 14.3 kW, the welding

Table 1 Chemical composition of the investigated materials in wt.-%

Material	Form	Element (%)								
		Fe	Cr	Ni	Mo	Mn	N	C	Si	P
Duplex AISI 2205	Base material	Bal.	22.96	5.18	3.00	1.82	0.17	0.02	0.29	0.03
Duplex AISI 2205	Powder	Bal.	22.80	5.57	3.16	1.09	0.16	0.02	0.68	0.02
Nickel	Powder	-	-	Bal.	-	-	-	0.05	-	-

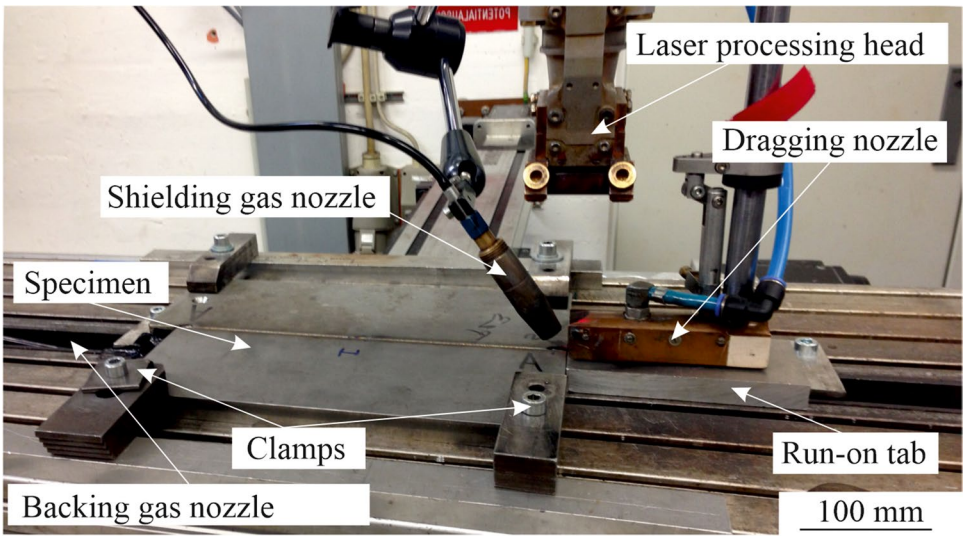

Fig. 2 Experimental setup for the laser beam welds

speed of 1.5 m·min^{-1} and a focal position of −5 mm. The experimental setup for the laser beam welding is shown in Fig. 2.

The quality of the weld seams was assessed by means of different destructive tests: The characterisation of the weld seams was done by cross-sections as well as electron backscatter diffraction (EBSD). Metallographic examinations were executed by grinding, polishing, etching of the specimen and light microscopy. The etching solution (Bloech and Wedl II) was applied according to [24] as this provides better possibility to distinguish between ferritic and austenitic phase. The amount of the phase constituents was determined from the cross-section by means of an optical image analysis software (Imagic IMS client, Imagic Bildverarbeitung).

The impact testing was done by means of sub-sized Charpy-V samples with a size of 7.5 mm × 10 mm × 55 mm. The specimens were taken out of the middle of the plate and tested at −20 °C. The notch was placed into the middle of the weld seam. Afterwards, the fractured surfaces were inspected by scanning electron microscope (SEM). Additionally, one piece was cut out of each broken specimen lengthwise to produce two cross-sections, one from the side and one from the middle of the specimen. Both cross-sections viewed the side of the fractured surface to determine the course of the fracture line (Fig. 3).

The corrosion resistance was tested accordingly to the ASTM G48 [25] method for pitting corrosion of stainless steels. The specimens were stored at 25 °C in a 6% $FeCl_3$ solution for 24 h; afterwards, they were weighted and examined at a 20× magnification. For both, impact and corrosion testing five specimens were welded with and without previous edge coating, respectively, were compared. For corrosion testing of the weld seams with previous edge coating, only four specimens were tested.

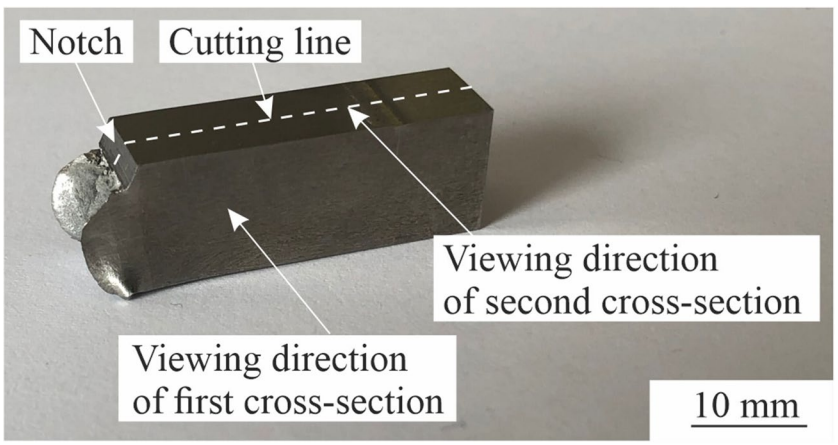

Fig. 3 Visualisation of cross-section extraction

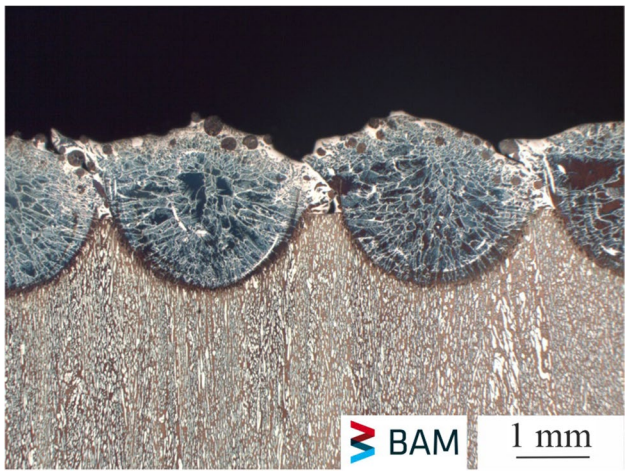

Fig. 4 Cross-section of coated edge with a stepover of 30%

3 Results and discussion

Cladded layers at the edges of the workpiece were produced with twenty single tracks. A stepover (distance between individual tracks) was taken as 60% of the track width of 1.6 mm. This stepover was chosen to produce as smooth edges as possible, thus minimising the gap between the joined parts for the subsequent laser beam welding process. If the DED tracks overlap was less by using a stepover of 30% of the track width, an unsatisfactory evenness of the coating occurs, as shown in the cross-section in Fig. 4. This results in a surface that is too wavy, which is unacceptable for the laser beam welding process, where only a very small gap between the joined parts can be tolerated. As the laser beam welding was carried out without any additional filler material, the waviness resulted in gaps between the joined parts, leading to underfilling on both sides of the weld.

A cross-section of the cladding is shown in Fig. 5a.

Optical analysis of the microstructure shows a uniform distribution of phases with approximately 50% austenite, which is attributed to the earlier transformation of ferrite to austenite due to the higher nickel content of the powder mixture, as shown in the phase diagram of v. Goldbeck [15]. The first tracks contain a higher proportion of the ferritic phase, presumably due to the initially cold base

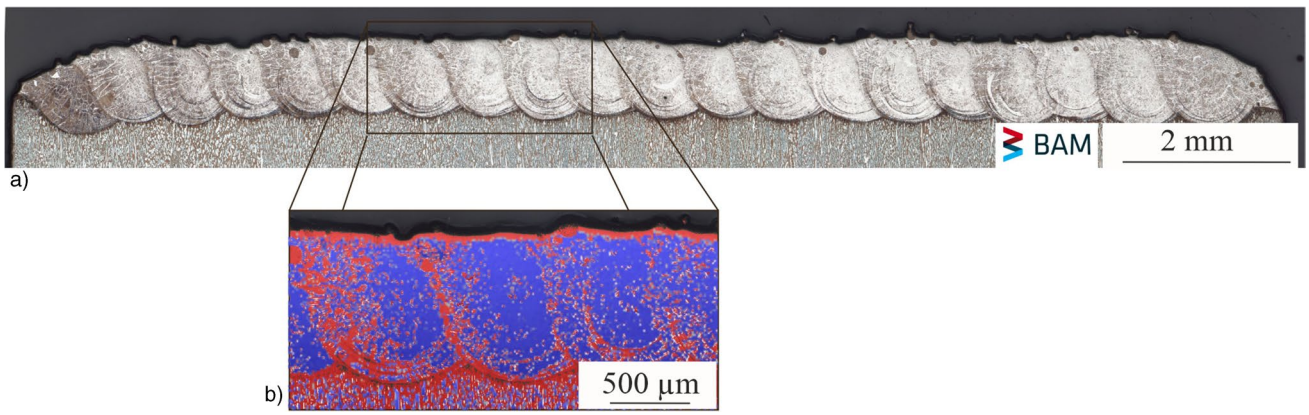

Fig. 5 Cross-section of coated edge (**a**); with ferritic phase coloured in red and austenitic phase in blue (**b**)

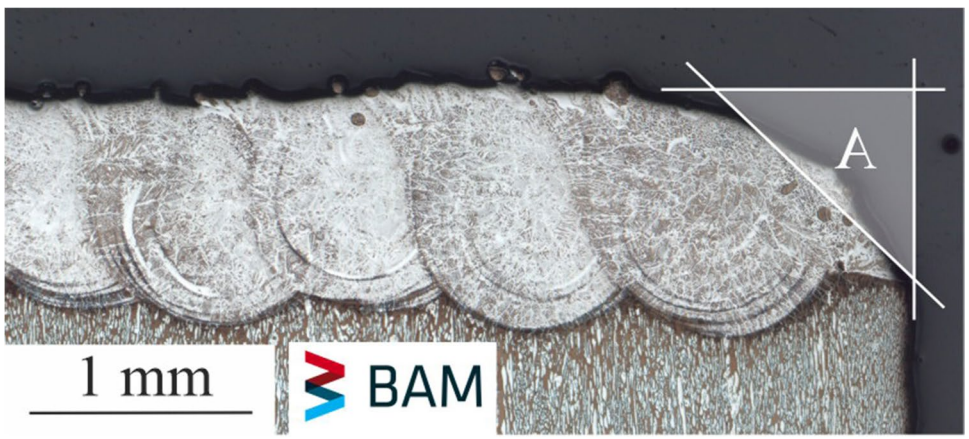

Fig. 6 Missing material in area A

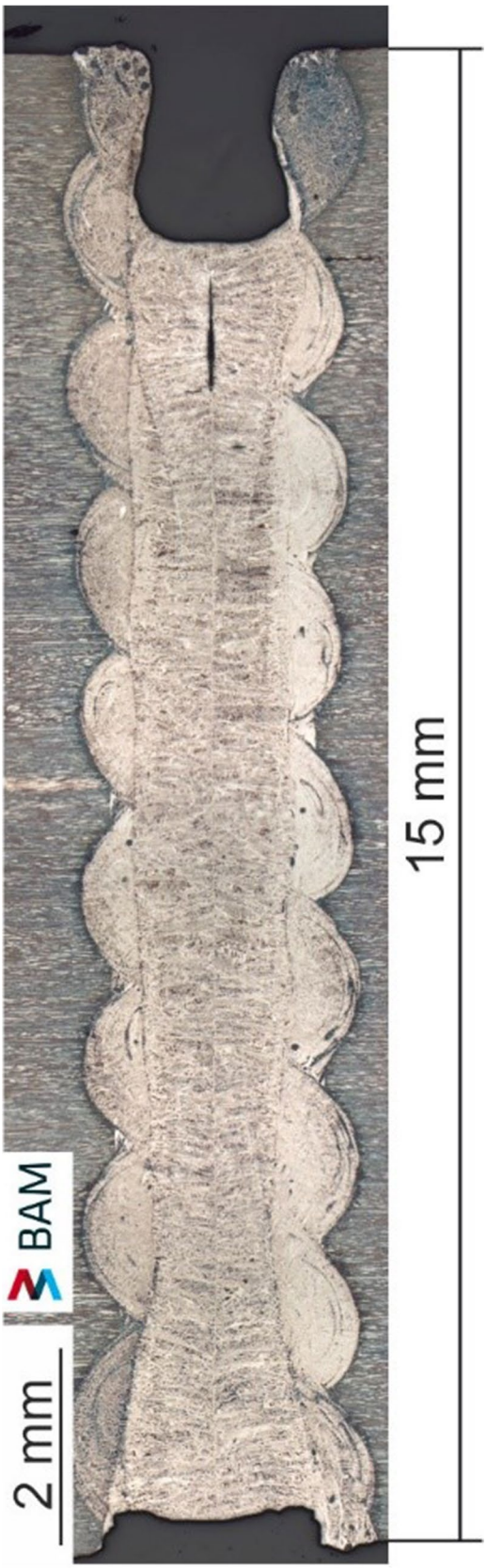

Fig. 7 Cross-sections of weld seam with underfilling and solidification crack

material, which heats up during the cladding process as the number of tracks increases. As described by Zambon and Bonollo [5], the longer $t_{12/8}$ time also has a positive effect on the formation of the austenitic phase, allowing an austenite ratio of about 50% compared to the shorter one for the first track with only 30% austenite.

The next problem that deals with the geometrical deviation of the coating is a material depletion at the first and last tracks that does not provide a perfect 90-degree angle at the edges of the base plate (the highlighted area A in Fig. 6).

Figure 7 shows a weld using conventional tack welding in three places using a laser beam, which does not provide any filler material to compensate for the missing volume. This results in significant underfilling as well as solidification cracks in the upper part of the laser weld. This type of crack is known to occur as a result of material shrinkage during solidification. The high cooling rates typical of laser beam welding, combined with the influence of the joint opening angle, which according to [26] results in higher plastic deformation just below the weld surface, could be a possible reason for the formation of solidification cracks. Material shrinkage combined with a high degree of restraint for this type of joint produces high tensile stresses or deformations that lead to separation of the liquid films between the dendrites, resulting in the formation of solidification cracks.

To compensate for the lack of material and to achieve defect-free welds, the influence of DED tracks instead of conventional tack welding was investigated. For this purpose, additional DED tracks were deposited on both sides of the weld joint prior to laser beam welding. The DED tracks along the entire length of the weld were used as tack welds to hold the parts together. This was done with the same parameters used for DED coatings.

Tack welds are essential to minimise distortion during welding. The additional time and effort required for DED tack welds is relatively small, even if such tracks are required on the top and root sides.

Figure 8 shows a photograph of a DED tack weld in plan view. Figure 9 shows an X-ray image of a DED tacked weld. The initial, the middle and the end parts of the welding specimen are areas, which were left free from the upper DED tack weld in oder to enable a seam tracking for the robot. These parts of the weld seam are marked in the X-ray image in Fig. 9. No defects were visible neither in the X-ray image nor in the cross-section of the weld shown in Fig. 13a. Thus, DED tack welding proves to be an effective solution to overcome solidification cracking and incomplete filling.

To further evaluate the microstructural constitution of different zones of the weld seams, an EBSD analysis and phase analysis by optical microscopy were done. Laser beam welds done without cladding or filler material were used as reference. Figure 10a shows a cross-section of such a weld seam. The ferritic phase, coloured in red

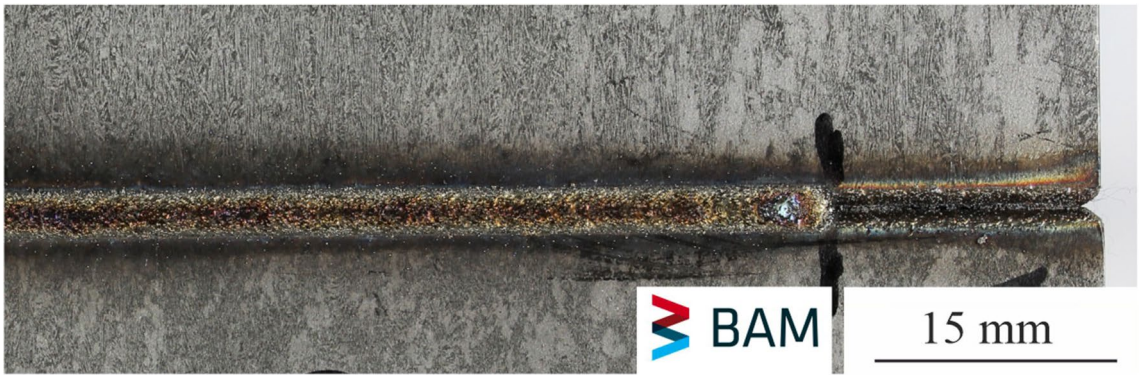

Fig. 8 Top view of plates with DED tacking before laser beam welding

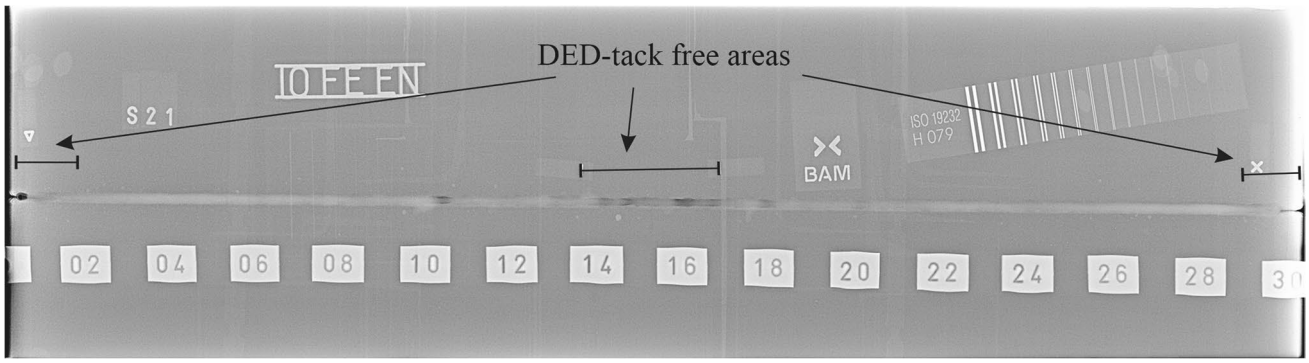

Fig. 9 X-ray image of weld seam with DED tacking

(Fig. 10b), displayed a ferrite content of about 90%. Even though nitrogen has been used as a shielding and backing gas following Lai et al. [14] and Muthupandi et al. [16], which should have positively influenced the formation of austenite, an unbalanced predominantly ferritic microstructure has been formed in the weld metal. Compared to their plates thickness (3 up to 6 mm), the specimen used here (15 mm) are far thicker and thus the influence of the nitrogen reduced to the upper and lower layer of the weld seam, where the austenite content is higher than in the middle, as shown in the magnification of the cross-sections.

Optical image analysis and EBSD measurements were done for the weld seams with prior DED coating. In Fig. 11, the positions of the regions of interest (ROI) analysed by EBSD are depicted. The cross-section shows a homogenous duplex microstructure throughout the whole depth of the weld seam. Compared to the welded joints with preplaced nickel foils investigated by Westin et al. [19] where a change of microstructure in the depth is shown, here the residual coating has appeared adjacent to the fusion line with a predominantly austenitic microstructure, which will be discussed in the following.

Figure 12a shows the phase distribution of the weld seam (ROI 1) with an average fraction of austenite (displayed in blue) of 55% that was also confirmed by optical analysis. This homogenous phase distribution was realised by the higher nickel content in the powder mixture previously applied on the plate's edges by DED clads.

The slight shift of the laser beam to one side of the weld seam (ROI 2, Fig. 12b) enables an evaluation of a region between the weld seam and residual coating located close to the base material. It shows a narrow predominantly austenitic band that represents the rest of the coating metal. The transition to the weld seam is smooth, while the transition to the base material is more distinct. With approx. 200 µm at the widest point, this transition area is quite slim and depicts the preferable positioning of coating and weld seam.

On the other side of the weld seam, ROI 3 (Fig. 12c) shows the transition of the austenitic residual coating to the duplex structure of the base material more obvious. Between both areas, a very narrow ferritic band is visible. This one is also detectable in the cross-section of the coating (Fig. 5) and may result from a reduced nickel content at the fusion

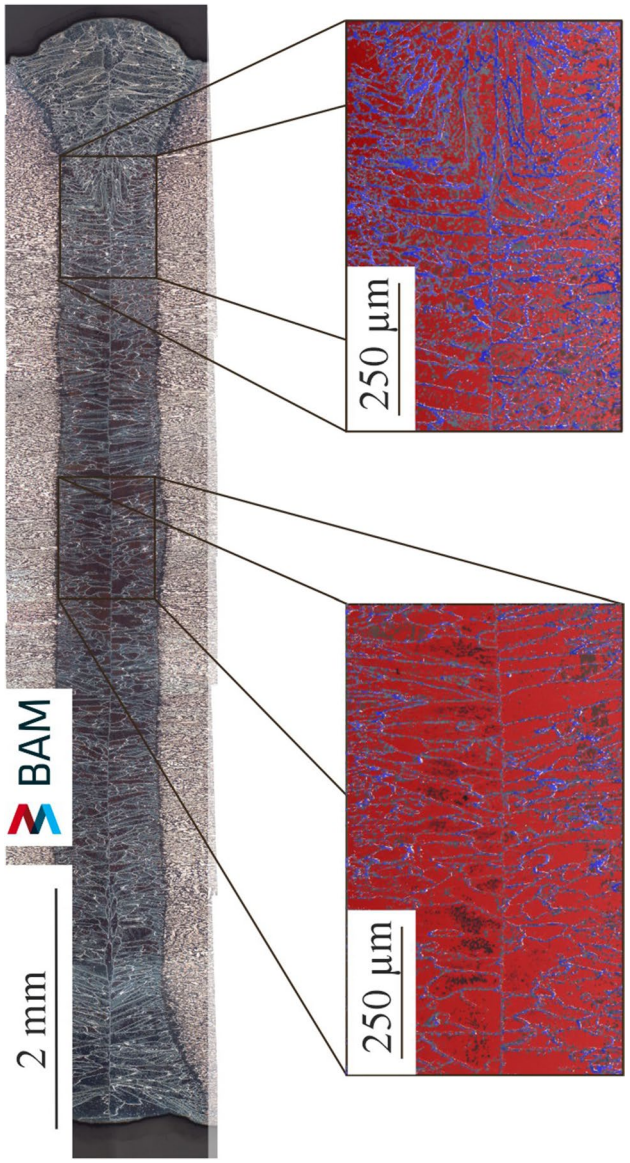

Fig. 10 Cross-section of weld seam without DED coating (**a**); with ferritic phase coloured in red and austenitic phase in blue (**b**)

line between coating to base material and thus a formation of a ferritic microstructure.

On this side of the weld seam, the coating is not completely molten during the laser beam welding process. The HAZ between the weld seam and the coating (ROI 3, Fig. 12d) is not distinct and can only be detected as a phase fraction shift from a balanced one in the seam to an almost complete austenitic in the residual coating. This is also the case in the previously discussed austenitic area in ROI 2.

The influence of the ferritic zone and the austenitic residual coating that might have an impact on the properties of the welded specimen were of particular interest. Charpy toughness tests were conducted on laser beam welded joints with previous DED coating as well as such without. The fracture surfaces of the broken specimen, both uncoated (Fig. 13a) and pre-coated ones (Fig. 13b), are exemplarily shown in Fig. 13, respectively, while the results of all tested specimen are listed in Table 2. Figure 13 (1–3) depicts SEM images of both fractured surfaces.

The welds without previous cladding showed a brittle fracture surface (Fig. 13a) that is not deformed and has a shiny crystalline appearance. This low impact toughness of average 29 J·cm^{-2} and the typical appearance of tear ridges in the SEM picture (Fig. 13 (1)) confirmed this, whereas weld joints with previous cladding showed a significant higher average impact toughness of 140 J·cm^{-2}. This, as well as the photograph of the broken specimen depicted in Fig. 13b, shows a more ductile fracture behaviour. The specimens were deformed plastically during the impact testing and the SEM pictures (Fig. 13 (2) and (3)) show a distinctive dimple structure. This can be attributed to the duplex microstructure with equal fractions of austenitic and ferritic phase. According to DIN EN 10088-2 [27], the minimum impact toughness for the duplex base material is 125 J·cm^{-2}, which all tested weld specimen (with exception of a single one with 123 J) reached. This provides evidence that the ferritic margin at the transition of residual coating to the base material has nearly no influence on the impact toughness. A closer look into the microstructure of the fractured surfaces and the course of the fracture line confirms this finding. Figure 14 displays the cross-sections of broken impact testing specimen of either position, the side view and from the middle. These two pictures are representative for all ten cross-sections and show the deformation of the weld seam and the residual coating as well as the notch and the fracture line. It is visible that no clear fracture zone can be determined. The rupture propagates through all areas: weld seam, residual coating and base material (Fig. 14a) and does not run along the transition of the coating to the base material. Figure 14b shows a cross-section where the fracture travels through the weld seam to the ferritic zone but deviates back into the weld seam again. In no specimen, the fracture line does run along a certain area but propagates through different ones. This does not allow for the statement that one area is more prone to brittle fracture than the other.

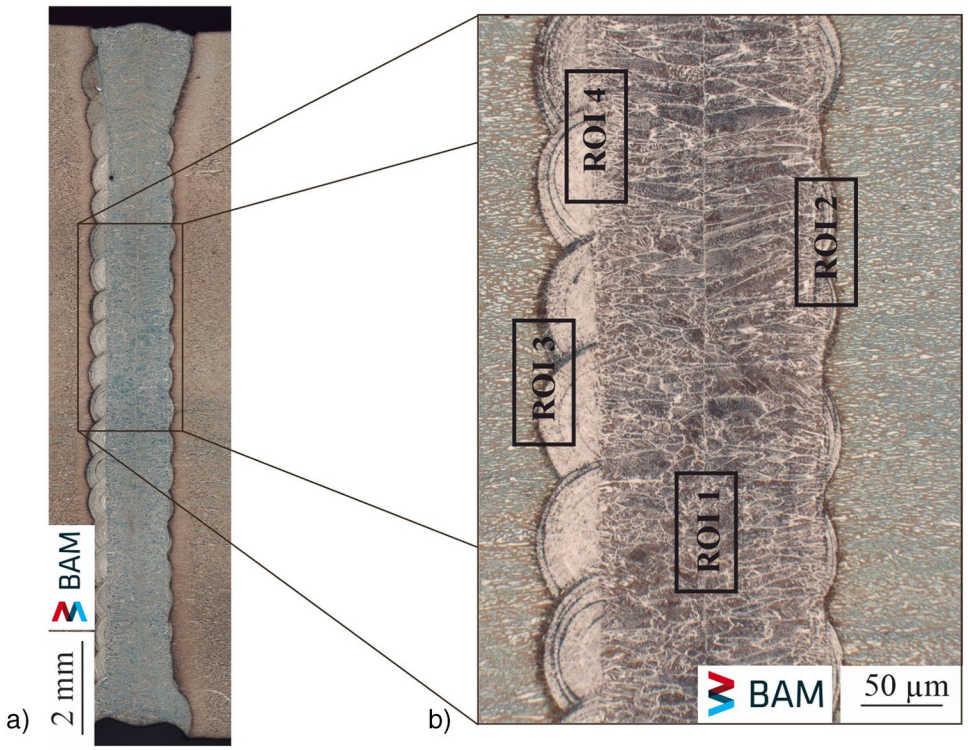

Fig. 11 Cross-section of weld seam (**a**) with regions of interest (**b**) for EBSD analysis

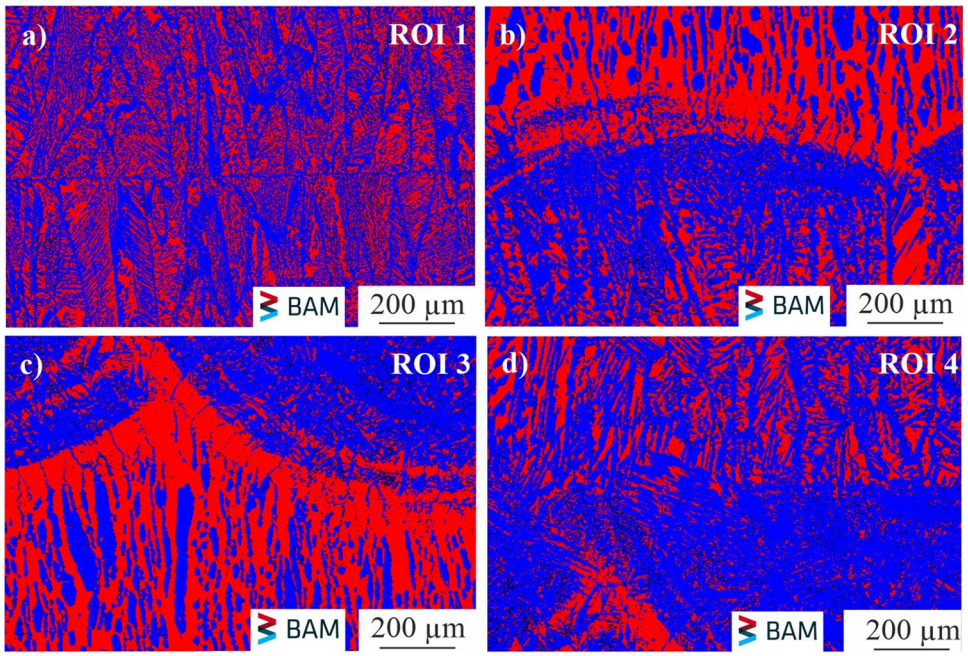

Fig. 12 EBSD of ROI 1 (**a**); ROI 2 (**b**); ROI 3 (**c**); ROI 4 (**d**) (blue colour—austenite, red—ferrite)

Another important aspect was the corrosion resistance of the weld seams. In combination with a good ductility, it is one of the major benefits of duplex stainless steels. The corrosion testing was done to cladded weld seams as well as those without cladding. Both cases are shown in Fig. 15. Additional to an optical inspection with a 20× magnification, the corrosion rate was calculated from the specimen weight before and after testing.

As expected, the weld seams with no coating showed pitting corrosion in all tested specimens, whereas the base metal was intact (Fig. 15a), as also reported by Westin et al. [19].

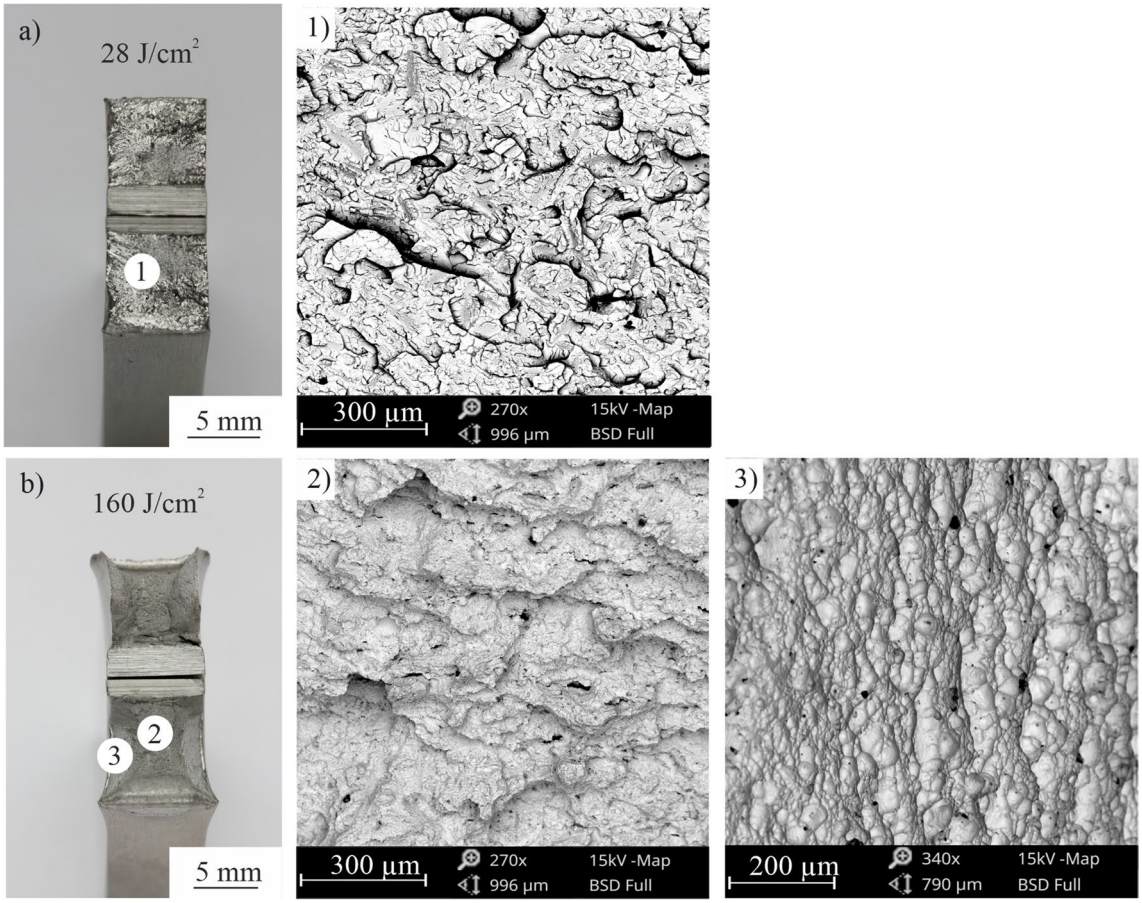

Fig. 13 Images of fractured surfaces of impact test specimens: uncoated specimen (**a**) with SEM image at marked position (1) and coated specimen (**b**) with SEM images at marked positions (2) and (3)

In comparison, two of the weld seams with pre-coated edges had a slight corrosive erosion at the transition of the residual coating to the base material. The other two had no defects at all, neither in the base metal of the plates nor in the weld seams (Fig. 15b). The corrosion rates (Table 3) confirm the impression of a good quality of the weld seams, as they are considerably higher for the specimens without DED-coated edges and according to ASTM A 923 [28], all except one specimen below the limit of 1 g·min^{-1}. In average, the corrosion rate has been improved by a factor four compared to the conventional welds.

Table 2 Results of impact testing (−20 °C) experiments of weld seams with and without previous cladding

Duplex 2205 uncoated edges		Duplex 2205 + Ni pre-coated edges	
Absorbed energy (KV) at −20 °C testing temperature in J	Impact toughness (A_k) in J·cm^{-2}	Absorbed energy (KV) at −20 °C testing temperature in J	Impact toughness (A_k) in J·cm^{-2}
17	28	83	136
16	26	98	160
26	42	88	144
14	23	75	123
16	26	84	137

4 Conclusions

A new approach to laser beam welding of thick duplex steel plates has been investigated. The two-step process presented, in which DED cladding was applied to the plate edges prior to welding, should be a viable alternative to achieve a balanced ratio of austenite and ferrite throughout the depth of the weld. Cladding was carried out using a powder mixture containing 12% nickel.

The lack of material due to the geometry of the claddings was compensated by tack welding with single DED tracks at the top and root of the weld.

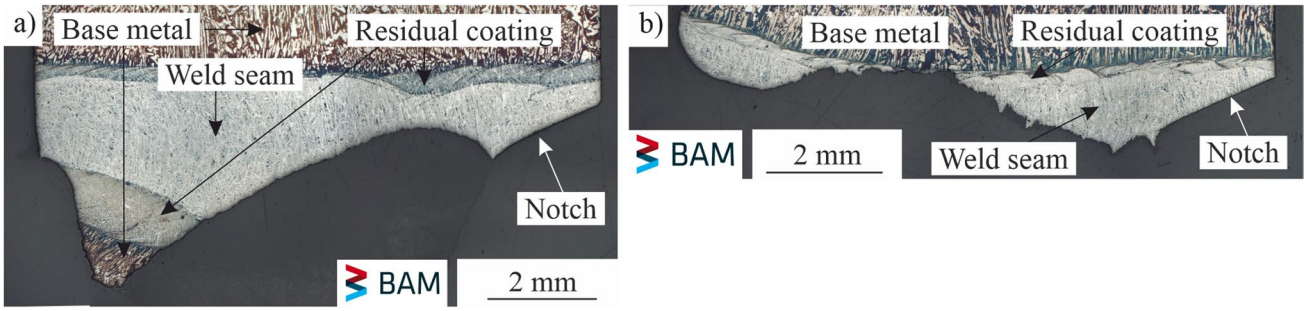

Fig. 14 Cross-section of broken impact testing specimens: from the side (**a**); from the middle (**b**)

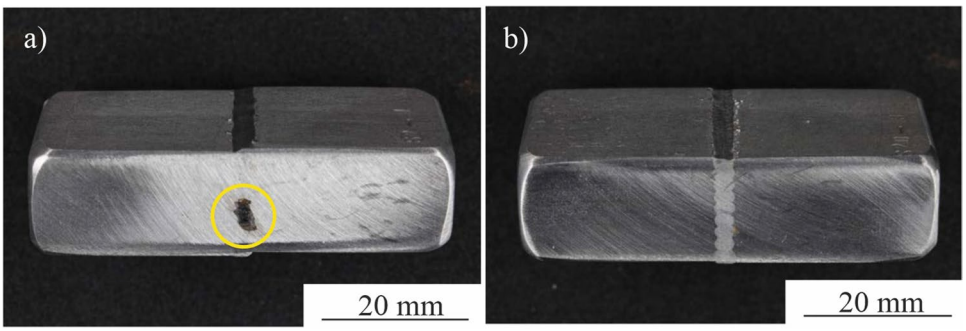

Fig. 15 Corrosion specimens: uncoated edges (**a**); coated specimen (**b**)

Table 3 Corrosion rates for weld seams with uncoated and coated edges

Corrosion rate in g·m^{-2} Duplex AISI 2205 — uncoated edges	Corrosion rate in g·m^{-2} Duplex AISI 2205 + Ni — coated edges
6.2 (p)	1.9 (p)
4.3 (p)	0.9 (p)
7.8 (p)	0.7 (n)
2.9 (p)	0.7 (n)
2.1 (p)	-

(p), trace of pitting detected; (n), no trace of pitting

Cross-sections and EBSD analysis showed a weld with a balanced microstructure, a HAZ with austenite in the residual cladding and a narrow ferritic band between the base material and the cladding.

Impact testing at −20 °C resulted in ductile fracture surfaces and higher impact toughness for the pre-coated specimen than for the uncoated welds, which showed a brittle fracture surface.

Corrosion tests performed an average four times lower corrosion rate for the pre-coated welds compared to conventional laser welds.

Acknowledgements The authors want to thank Butting GmbH and personally Mr. M. Schlundt kindly for providing the base material as well as for performing the corrosion testing. Additionally, the authors want to thank Mr. M. Grunwald (Department 8.3 — Radiological Methods, BAM) for conducting the X-ray analysis and Mr. R. Saliwan Neumann (Department 5.1 — Materialography, Fractography and Ageing of Engineered Materials, BAM) for the EBSD measurement.

Funding Open Access funding enabled and organized by Projekt DEAL. This work was supported by the Federation of Industrial Research Association (AiF, project number 19.228N) and the German Federal Ministry for Economic Affairs and Energy (BMWi—Bundesministerium für Wirtschaft und Energie) based on a resolution of the Deutscher Bundestag.

Declarations

Conflict of interest The authors declare no competing interests.

References

1. Charles J (2008) Duplex stainless steels — a review after DSS '07 held in Grado. Steel Res Int 79:455–465. https://doi.org/10.1002/srin.200806153
2. Kotecki DJ (1986) Ferrite control in duplex stainless steel weld metal. Weld Res Suppl 10:273–278
3. Hoffmeister H, Lothongkum G (1994) Effects of chemical composition of duplex stainless steels on microstructure and pitting corrosion after solution heat treatment and various weld simulation cooling cycles. Weld World 33:91–96
4. Arun D, Devendranath Ramkumar K, Vimala R (2019) Multi-pass arc welding techniques of 12 mm thick super-duplex stainless steel. J Mater Process Technol 273:126–143. https://doi.org/10.1016/j.jmatprotec.2019.03.031
5. Zambon A, Bonollo F (1994) Rapid solidification in laser welding of stainless steels. Mater Sci and Eng: A 178:203–207. https://doi.org/10.1016/0921-5093(94)90544-4
6. Capello E, Castelnuovo M, Previtali B, Vedani M (2004) Laser surface treatment of laser welded duplex stainless steel. In: Proc of the 34th Int MATADOR Conference, London. https://doi.org/10.1007/978-1-4471-0647-0_39
7. Young MC, Tsay LW, Shin CS, Chan SLI (2007) The effect of short time post-weld heat treatment on the fatigue crack growth of 2205 duplex stainless steel welds. International J of Fatigue 29:2155–2162. https://doi.org/10.1016/j.ijfatigue.2007.01.004
8. Muthupandi V, Srinivasan P, Seshadri SK, Sundaresan S (2003) Effect of weld metal chemistry and heat input on the structure and properties of duplex stainless steel welds. Mater Sci and Eng: A 358:9–16. https://doi.org/10.1016/S0921-5093(03)00077-7
9. Deng B, Wang Z, Jiang Y, Sun T, Xu J, Li J (2009) Effect of thermal cycles on the corrosion and mechanical properties of UNS S31803 duplex stainless steel. Corros Sci 51:2969–2975. https://doi.org/10.1016/j.corsci.2009.08.015
10. Nilsson JO (1992) Super duplex stainless steels. Mater Sci Technol 8:685–700. https://doi.org/10.1179/mst.1992.8.8.685
11. van Nassau L, Meelker H, Hilkes J (1992) Welding duplex a super duplex stainless steels—a guide. Weld World 31:322–343
12. Keskitalo M, Mäntyjärvi K, Sundqvist J, Powell J, Kaplan AFH (2015) Laser welding of duplex stainless steel with nitrogen as shielding gas. J Mater Process Technol 216:381–384. https://doi.org/10.1016/j.jmatprotec.2014.10.004
13. Baghdadchi A, Hosseini VA, Hurtig K et al (2021) Promoting austenite formation in laser welding of duplex stainless steel—impact of shielding gas and laser reheating. Weld World 65:499–511. https://doi.org/10.1007/s40194-020-01026-7
14. Lai R, Cai Y, Wu Y, Li F, Hua X (2016) Influence of absorbed nitrogen on microstructure and corrosion resistance of 2205 duplex stainless steel joint processed by fiber laser welding. J Mater Process Technol 231:397–405. https://doi.org/10.1016/j.jmatprotec.2016.01.016
15. von Goldbeck OK (1982) Iron—nickel Fe—Ni. In: von Goldbeck OK (ed) IRON—binary phase diagrams, 1st edn. Springer, Berlin, Heidelberg, pp 73–79
16. Muthupandi V, Bala Srinivasan P, Shankar V, Seshadri SK, Sundaresan S (2005) Effect of nickel and nitrogen addition on the microstructure and mechanical properties of power beam processed duplex stainless steel (UNS 31803) weld metals. Mater Lett 59:2305–2309. https://doi.org/10.1016/j.matlet.2005.03.010
17. Wu HC, Tsay LW, Chen C (2004) Laser beam welding of 2205 duplex stainless steel with metal powder additions. ISIJ International 44:1720–1726. https://doi.org/10.2355/isijinternational.44.1720
18. Gook S, Gumenyuk A, Rethmeier M (2014) Hybrid laser arc welding of X80 and X120 steel grade. Science and Technology of Welding and Joining 19:15–24. https://doi.org/10.1179/1362171813Y.0000000154
19. Westin EM, Stelling K, Gumenyuk A (2011) Single-pass laser-GMA hybrid welding of 13.5 mm thick duplex stainless steel. Weld World 55:39–49. https://doi.org/10.1007/BF03263514
20. Birger EM, Moskvitin GV, Polyakov AN, Arkhipov VE (2011) Industrial laser cladding: current state and future. Weld Int 25:234–243
21. Rottwinkel B, Nölke C, Kaierle S, Wesling V (2014) Crack repair of single crystal turbine blades using laser cladding technology. Procedia CIRP 22:263–267. https://doi.org/10.1016/j.procir.2014.06.151
22. Meng W, Xiaohui Y, Zhang W, Junfei F, Lijie G, Qunshuang M, Bing C (2020) Additive manufacturing of a functionally graded material from Inconel625 to Ti6Al4V by laser synchronous preheating. J Mater Process Technol 275:116368. https://doi.org/10.1016/j.jmatprotec.2019.116368
23. Straße A, Gumenyuk A, Rethmeier M (2022) Study on duplex stainless steel powder compositions for the coating of thick plates for laser beam welding. Adv Eng Mater 24:2101327. https://doi.org/10.1002/adem.202101327
24. Weck E, Leistner E (1986) Metallographische Anleitung zum Farbätzen nach dem Tauchverfahren - Teil III: Nichteisenmetalle. Nickel-Basis-und Kobalt-Basis-Legierungen, Deutscher Verlag für Schweißtechnik (DVS) GmbH, Düsseldorf, Hartmetalle und Eisenwerkstoffe
25. ASTM G48-11 (2015) Standard test methods for pitting and crevice corrosion resistance of stainless steels and related alloys by use of ferric chloride solution. ASTM International
26. Weise S (1998) Heißrissbildung beim Laserstrahlschweißen von Baustählen. Dissertation,. Universität Bremen, Aachen
27. DIN EN (2014) 10088-2:2014 Nichtrostende Stähle – Teil 2: Technische Lieferbedingungen für Blech und Band aus korrosionsbeständigen Stählen für allgemeine Verwendung. Deutsche Fassung EN 10088-2:2014
28. ASTM A 923-03 (2014) Standard test methods for detecting detrimental intermetallic phase in duplex austenitic/ferritic stainless steels. ASTM International